Available online at www.sciencedirect.com
SCIENCE DIRECT®
Journal of the European Ceramic Society 25 (2005) 1397–1403
www.elsevier.com/locate/jeurceramsoc

Three-dimensional observation of the entangled eutectic structure in the Al_2O_3–YAG system

Hideyuki Yasuda [a,*], Itsuo Ohnaka [a], Yoshiki Mizutani [a,1], Takashi Morikawa [a], Satoshi Takeshima [a], Akira Sugiyama [a], Yoshiharu Waku [b], Akira Tsuchiyama [c], Tsukasa Nakano [d], Kentaro Uesugi [e]

[a] Department of Adaptive Machine Systems, Osaka University, Suita, Osaka 565-0871, Japan
[b] Ube Research Laboratory, Corporate Research and Development, UBE Industries, Ltd., Ube, Yamaguchi 755-8633, Japan
[c] Department of Earth and Space Science, Osaka University, Osaka 560-0043, Japan
[d] Geological Survey of Japan, National Institute of Advanced Industrial Science and Technology, Tsukuba 305-8567, Japan
[e] Japan Synchrotron Radiation Research Institute, Hyogo 679-5198, Japan

Available online 15 February 2005

Abstract

The coupled growth zone of the Al_2O_3–YAG eutectic system was examined by means of high resolution X-ray tomography. The entangled eutectic structure was observed for the unidirectional solidification and the solidification from the undercooled melt at the equilibrium eutectic composition (Al_2O_3–18.5 mol% Y_2O_3). The reconstructed three-dimensional images showed that both the Al_2O_3 and the YAG phases branched and that the entangled domain was of the same order as the lamellar spacing. Comparison of the branching in the Al_2O_3–YAG eutectic system to that in metallic alloys that exhibit the regular or the irregular eutectic structure indicated that the frequent branching of both phases resulted in the entangled structure.

Keywords: Eutectic; Non-destructive evaluation

1. Introduction

It has been reported that unidirectionally solidified Al_2O_3-based eutectic composites have excellent mechanical properties at high temperatures.[1–9] For example, Al_2O_3–YAG ($Y_3Al_5O_{12}$, yttrium-aluminum-garnet) eutectic composites exhibit flexural strengths of 360–500 MPa from room temperature to 2073 K in an air atmosphere.[5] The compression creep strength at 1873 K is about 13 times higher than that of sintered composites with the same chemical compositions.[6] Therefore, because of their mechanical properties, eutectic ceramics such as Al_2O_3–YAG are candidates for high temperature use.

In the eutectic composites, it has been reported that the constituent phases with faceted interfaces are three-dimensionally continuous and are complexly entangled with each other without grain boundaries.[5,8,9] Eutectic structures are highly textured with two twin-related crystallographic orientations.[10] Since the mechanical properties are closely related to the entangled structure, it is of interest to investigate the eutectic solidification of the Al_2O_3–YAG system.

One of the characteristics of the Al_2O_3–YAG eutectic solidification is a narrow coupled growth zone.[11,12] The eutectic structure without any primary phase was obtained only at compositions ranging from Al_2O_3–18.5 mol% Y_2O_3 (the Al_2O_3–YAG eutectic composition is 18.5 mol% Y_2O_3) to 20.5 mol% Y_2O_3 for the unidirectional solidification and the solidification from the undercooled melt.

Another characteristic is the Al_2O_3–YAG eutectic solidification accompanied by the melting of the Al_2O_3–YAP metastable eutectic structure.[13,14] Solidification in the

* Corresponding author. Tel.: +81 6 6879 7475; fax: +81 6 6879 7476.
E-mail address: yasuda@ams.eng.osaka-u.ac.jp (H. Yasuda).
[1] Present address: National Institute of Advanced Industrial Science and Technology, Nagoya 463-8560, Japan.

0955-2219/$ – see front matter © 2005 Elsevier Ltd. All rights reserved.
doi:10.1016/j.jeurceramsoc.2005.01.019

Al_2O_3–YAP ($YAlO_3$, yttrium-aluminum-perovskite) metastable eutectic path normally occurs when the melt is heated up to a temperature above 2273 K once.[15–18] The Al_2O_3–YAP metastable eutectic structure melted when the specimen was heated up to the metastable eutectic temperature.[13] The solidification of the Al_2O_3–YAG equilibrium eutectic system immediately followed the melting of the Al_2O_3–YAP metastable eutectic system, resulting in the fine eutectic structure. It was pointed out that shape casting was performed using the solidification accompanying the melting.[14]

Three-dimensional observation is useful for investigating the eutectic growth mechanism, since the time evolution of the eutectic structure during the unidirectional solidification is expected to remain in the growth direction. Micro X-ray tomography using the synchrotron radiation facility has been developed, in which the spatial resolution is in the order of μm.[19,20] First, this paper briefly summarizes the coupled growth of the Al_2O_3–YAG. Then, the three-dimensional observations obtained by the micro X-ray tomography are presented. On the basis of the three-dimensional observations, evolution of the entangled eutectic structure is discussed.

2. Experiments

2.1. Solidification procedure

Specimens for the unidirectional solidification were prepared using 99.99% α-Al_2O_3 and 99.9% Y_2O_3 powders. The temperature gradient measured by pyrometers was roughly 10^4 K/m. The Mo crucible used was 8 mm in outer diameter, 5 mm in inner diameter and 75 mm in depth. Details of the unidirectional experiment are given in the previous work.[11] Solidification in the undercooled melt and solidification of the Al_2O_3–YAG eutectic system accompanied by the melting of the Al_2O_3–YAP metastable eutectic structure were examined using an optical DTA apparatus.[12,21]

The Al_2O_3–YAG eutectic spacing was numerically estimated from the interfacial length (interface between Al_2O_3 and YAG) per unit area.[14] The interfacial length per unit area, L, was estimated from transverse sections (500 μm × 500 μm) using an image analyzer. The lamellar spacing was simply estimated by $2/L$. In an ideal lamellar structure in which the lamellar phases are perfectly aligned, the estimated value strictly coincides with the lamellar spacing.

2.2. X-ray tomography

The experiments were performed at the micro X-ray computerized tomography (micro X-ray CT) facility of beam line BL47XU in SPring8.[19] An "in-vacuum type" undulator was employed as an X-ray source, and the radiation was monochromatized with a Si(1 1 1) double crystal monochromator. The cross-section of the monochromatic X-ray beam was about 2 mm × 1 mm at 50 m from the light source (around the sample position). This highly collimated undulator radiation from the low emittance storage ring is very suitable for high spatial resolution tomography.

Transmission X-ray images were obtained using a beam monitor (BM) for X-rays (BM AA50, Hamamatsu Photonics K.K.) and a CCD camera (C4880-10-14A, Hamamatsu Photonics K.K.). The beam monitor consists of a single crystal phosphor screen (Lu_2SiO_5) and a microscope objective. The format of the CCD camera is 1000 × 1018 pixels. In the transmitted images, the effective pixel size is 0.5 μm × 0.5 μm. The transmitted image was recorded as a 14 bit-depth image. The exposure time for every transmitted image was 1.5 s. The distance between the sample and the phosphor screen was set as small as possible to avoid artifacts due to the phase contrast image. A high precision rotation stage with an air bearing was used for sample rotation. The convolution back projection method was used for the tomographic reconstruction.

Al_2O_3–YAG eutectic specimens grown at a growth rate of 1.4×10^{-7} m/s were used for the micro X-ray CT. Specimens with dimensions of 200 μm × 200 μm × 1 mm were prepared from the unidirectionally solidified ingots. An X-ray beam of 25 keV was used to obtain the transmitted images with sufficient contrast.

3. Results and discussion

3.1. Microstructure of the Al_2O_3–YAG eutectic system

Two types of eutectic structures were observed in the Al_2O_3–YAG eutectic system. One was the entangled eutectic structure shown in Fig. 1(a) and (b). The entangled eutectic structure was obtained when the Al_2O_3–YAG eutectic specimens (18.5 mol% Y_2O_3) were unidirectionally solidified at growth rates ranging from 10^{-7} to 10^{-5} m/s.[11] The entangled eutectic structure with narrower lamellar spacing was also obtained when the specimens (18.5 mol% Y_2O_3) solidified in the undercooled melts. In the solidification in the undercooled melts, the degree of the nucleation undercooling was 100 K at most and the growth rate ranged from 5×10^{-5} to 2×10^{-4} m/s.[12]

The other eutectic structure, in which the Al_2O_3 phase with the rod or the lamellar shape is distributed in the YAG phase and the two phases are not entangled, was observed at a composition of 22.5 mol% Y_2O_3 (Al_2O_3–YAP metastable eutectic composition).[13] The eutectic structure was produced when the Al_2O_3–YAP metastable eutectic structure melts at the metastable eutectic temperature and the Al_2O_3–YAG equilibrium eutectic structure were generated concurrently.[13,22] In this solidification process, the exothermic heat due to the solidification is coupled with the endothermic heat due to the melting, resulting in higher growth rates.[22] Thus, the coupled growth mechanism that resulted in the entangled structure did not operate at the higher growth rate for the off-eutectic specimen.

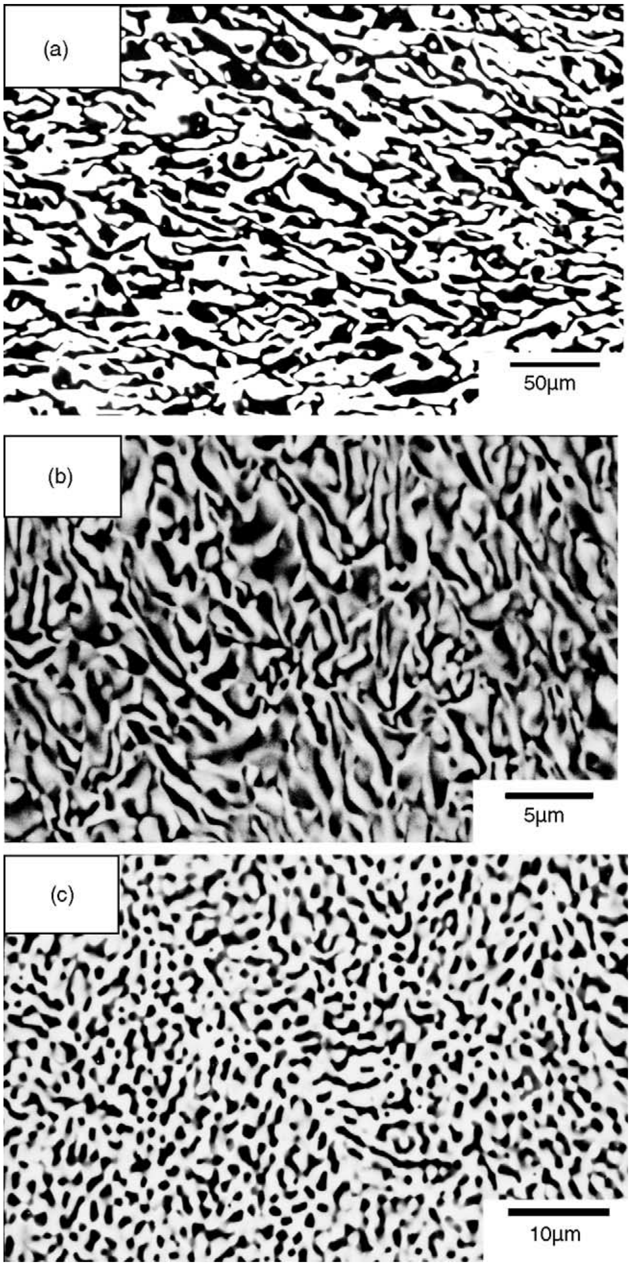

Fig. 1. Microstructures of Al_2O_3–YAG equilibrium eutectic system. (a) Longitudinal section of the unidirectionally solidified Al_2O_3–18.5 mol% Y_2O_3 specimen (1.4×10^{-7} m/s), (b) Al_2O_3–18.5 mol% specimen solidified from the undercooled melt at a cooling rate of 1 K/s, (c) Al_2O_3–YAG equilibrium eutectic structure (Al_2O_3–22.5 mol% Y_2O_3) produced by melting the Al_2O_3–YAP metastable eutectic structure above the metastable eutectic temperature and below the equilibrium eutectic temperature. The black and the white phases are α-Al_2O_3 and YAG, respectively.

Fig. 2 shows the lamellar spacing as a function of growth velocity.[22] The lamellar spacing of the μ-PD method in which a rod-shaped crystal was pulled down from a hole in the bottom of the platinum crucible[23] was also plotted. For both of the eutectic structures, the eutectic spacing roughly obeys the relationship $\lambda^2 V = A$ (A: constant) derived from the Jackson–Hunt coupled growth model.[24]

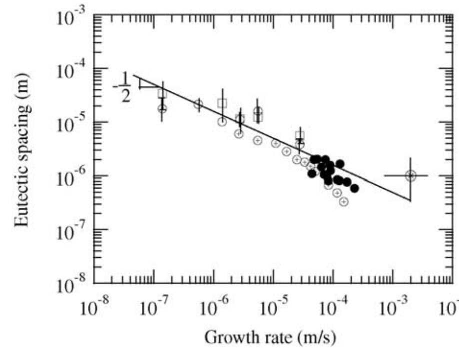

Fig. 2. Lamellar spacing of the solidification of the equilibrium eutectic structure accompanied by the melting of the metastable eutectic structure in the heating procedure (⊗). Lamellar spacing of the unidirectional solidification ((◯) 18.5 mol% Y_2O_3, (☐) 20.5 mol% Y_2O_3) [11], μ-PD method (⊕) [23] and solidification from the undercooled melt (●) [12] are also plotted.

The coupled growth mechanism resulting in the entangled eutectic structure operated over a wide growth rate range (10^{-7} to 10^{-4} m/s). In this study, the specimen (18.5 mol% Y_2O_3) solidified at a lower growth rate of 1.4×10^{-7} m/s was used for the X-ray tomography, since the spatial resolution of the tomography has to be sufficiently high in comparison to the eutectic lamellar spacing.

3.2. X-ray tomography of the Al_2O_3–YAG eutectic structure

Fig. 3(a) shows the reconstructed images of the unidirectionally solidified Al_2O_3–YAG eutectic structure (Al_2O_3–18.5 mol% Y_2O_3). The images are perpendicular to the growth direction. All reconstructed images are similar to each other, since there is no distinction between the characteristics of the entangled structures (i.e. direction of the lamellae, lamellar spacing). The X-ray analysis revealed a crystallographic orientation relationship between the Al_2O_3 and the YAG phases, as shown in Fig. 3(b). The specimen used for the CT consisted of α-Al_2O_3 and YAG single crystals, since the X-ray diffractions are consistently identified on the basis of the single crystallographic domain. The following relationship for the crystallographic orientation between the two phases was obtained.

$$(0\,0\,0\,1)_{Al_2O_3} || (1\,\bar{1}\,2)_{YAG},\ [\bar{1}\,1\,0\,0]_{Al_2O_3} || [1\,\bar{1}\,\bar{1}]_{YAG}.$$

This relationship coincides with that in the earlier work.[10] The present specimen did not contain the twin-related orientations.

In the reconstructed images as shown in Fig. 3(a), the lamellae tended to align in a certain direction. However, comparison between the lamellae in the reconstructed images and the crystallographic orientations indicated that the lamellar alignment was not predominantly determined by the crystallographic orientations. Fig. 3(c) shows the normal vectors of the interface between the Al_2O_3 and the YAG phases. Although the normal vectors are slightly segregated in the

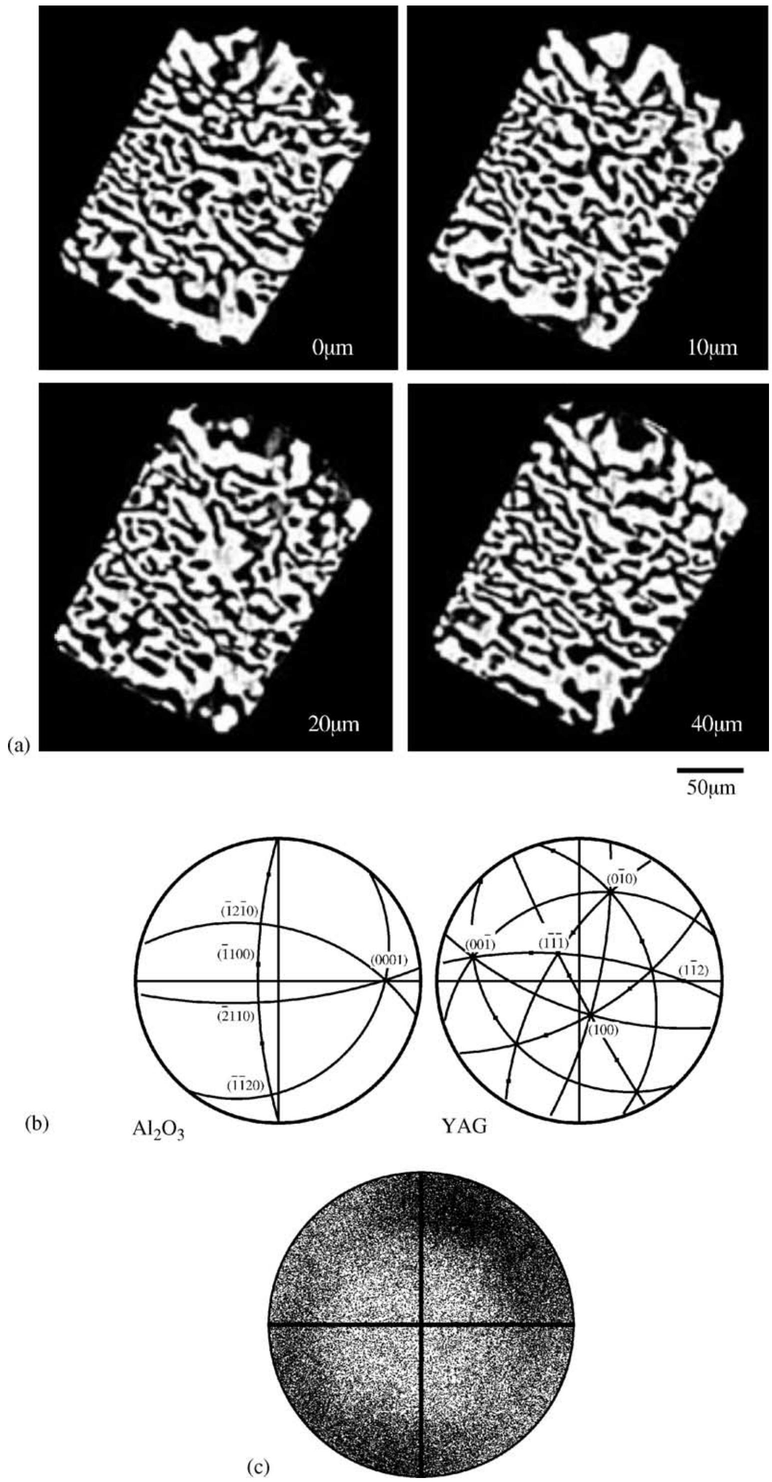

Fig. 3. (a) Reconstructed images of the unidirectionally solidified Al_2O_3–YAG eutectic structure (Al_2O_3–18.5 mol% Y_2O_3) perpendicular to the growth direction. Numbers indicate the relative growth length. Black is α-Al_2O_3 and white is YAG. (b) Stereographic projections of α-Al_2O_3 and YAG, and (c) stereographic projection of the normal vectors of the interface between α-Al_2O_3 and YAG.

upper-right or the lower-left regions due to the lamellar alignment observed in Fig. 3(a), they are widely distributed. Comparison of the normal vectors and the crystallographic orientations suggests that the interface between the Al_2O_3 and the YAG phases does not have definite crystallographic planes on a macroscopic scale.

Fig. 4 shows the three-dimensional image of the Al_2O_3–YAG eutectic structure constructed from the reconstructed images as shown in Fig. 3(a). The growth morphology continuously changed, keeping the characteristic feature in the entangled structure. Entangling in the growth direction frequently occurred and the entangled domain was of the same order as the lamellar spacing. The three-dimensional image clearly indicates that the eutectic growth in the Al_2O_3–YAG system was far from the steady state.

The entangled part in the Al_2O_3–YAG eutectic structure is shown in Fig. 5(a). A hole is observed in the central part of Fig. 5(a), indicating that the Al_2O_3 phase pierces through the YAG phase. Fig. 5(b) shows the slice images perpendicular to the growth direction. Morphological change in the growth direction gives time evolution of the entangled structure during the unidirectional solidification. Branching of the YAG phase (black phase) occurred from image C to image D. In other words, the Al_2O_3 phase grew over the YAG phase. From image E to image F, opposite branching of the Al_2O_3 phase occurred at almost the same position on the transverse cross section. As a result of the sequential branching of the YAG and the Al_2O_3 phases at the same position on the transverse plane, the Al_2O_3 phase pierces through the YAG phase. The distance between the YAG branching and the Al_2O_3 branching is approximately 20 μm, while the lamellar spacing is 10 μm.

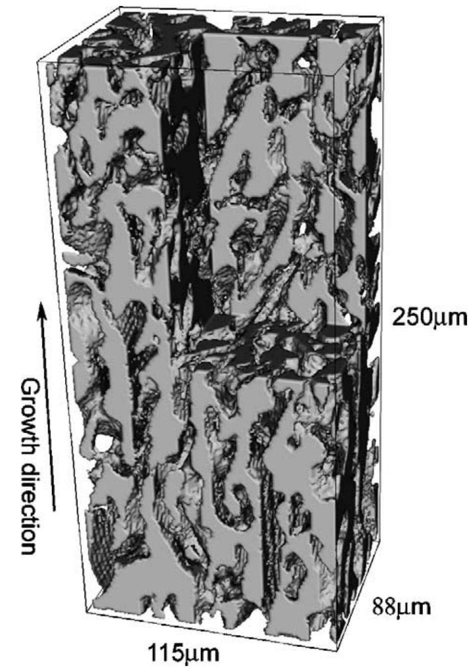

Fig. 4. Three-dimensional image of the unidirectionally solidified Al_2O_3–YAG eutectic structure (Al_2O_3–18.5 mol% Y_2O_3). The α-Al_2O_3 phase was removed from the image.

The eutectic structures are classified by considering the branching sequence. The regular eutectic structure, in which a minor phase with a lamellar or rod shape regularly aligns

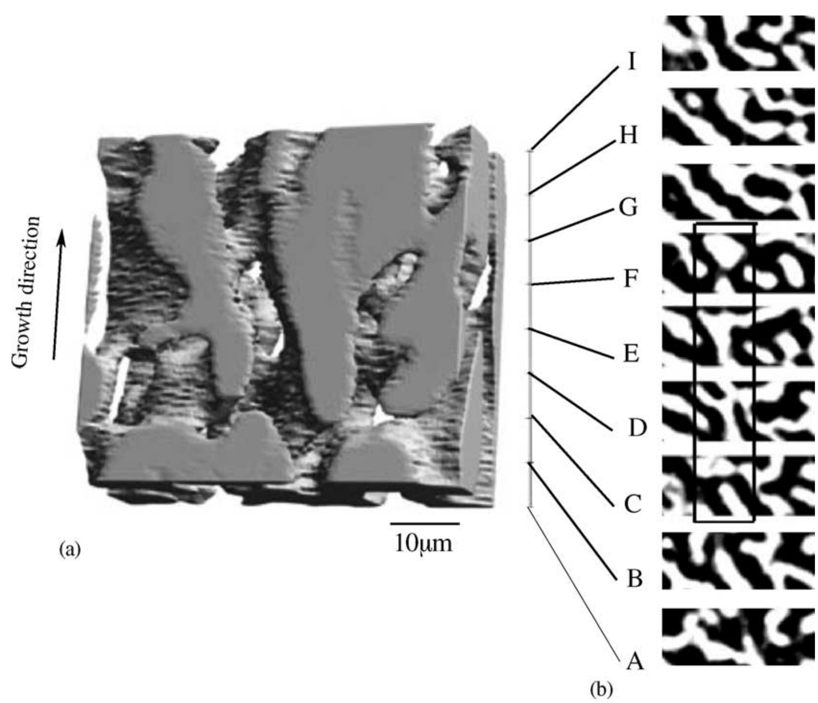

Fig. 5. (a) Three-dimensional image of the YAG phase in the entangled region and (b) sequence of the slice images perpendicular to the growth direction. Black and white phases are YAG and Al_2O_3, respectively.

parallel to the growth direction, is observed for many metallic alloy systems with non-faceted interfaces.[24–27] In the Sn–Pb eutectic system, which exhibits the regular eutectic structure, X-ray tomography showed that the branching frequency is extremely low in comparison with the Al_2O_3–YAG system.[28] The continuous growth of the Sn-rich and Pb-rich phases results in the regular eutectic structure. In the Sn–Bi eutectic system that exhibits the irregular eutectic structure,[25–30] the Sn-rich phase hardly branches and the Bi phase with a faceted interface branches frequently.[28] The branching of only the Bi phase results in the irregular eutectic structure. The hole shown in Fig. 5(a) is not produced by single phase branching. The sequential branching of both phases at the same transverse section produces the hole, and the frequent branching results in the entangled structure.

4. Conclusion

The entangled structure of the Al_2O_3–YAG equilibrium eutectic system was observed in the unidirectional solidification and the solidification from the undercooled melt. The growth rate that produced the entangled structure at the equilibrium eutectic composition (18.5 mol% Y_2O_3) ranged from 10^{-7} to 10^{-4} m/s. The entangled eutectic structure grown at 1.4×10^{-7} m/s was studied by micro X-ray tomography. Comparison of the lamellae in the reconstructed images to the crystallographic orientations indicated that the lamellar alignment was not predominantly determined by the crystallographic orientations. In addition, the interface between the two phases did not have a definite crystallographic relationship. Both the Al_2O_3 and the YAG phases branched at the same position on the transverse section. The entangled domain is of the same order as the lamellar spacing. The frequent branching of the two phases resulted in the entangled structure.

Acknowledgments

The authors thank Dr. K. Tanaka at Kagawa University for supporting the crystal orientation analysis. The synchrotron radiation experiments were performed at the BL47XU in the SPring-8 with the approval of the Japan Synchrotron Radiation Research Institute (JASRI). This work is supported in part by a Grant-in-Aid for Scientific Research and the 21st Century COE Program given by the Ministry of Education, Culture, Sports, Science and Technology, Japan. This work is partially supported by New Energy and Industrial Technology Development Organization (NEDO).

References

1. Mah, T. and Parthasarathy, T. A., Processing and mechanical properties of $Al_2O_3/Y_3Al_5O_{12}$ (YAG) eutectic composite. *Ceram. Eng. Sci. Proc.*, 1990, **11**, 1617–1627.
2. Parthasarathy, T. A. and Mah, T., Creep behavior of an Al_2O_3–$Y_3Al_5O_{12}$ eutectic composite. *Ceram. Eng. Sci. Proc.*, 1990, **11**, 1628–1638.
3. Parthasarathy, T. A. and Mah, T., Deformation behavior of an Al_2O_3–$Y_3Al_5O_{12}$ eutectic composite in comparison with sapphire and YAG. *J. Am. Ceram. Soc.*, 1993, **76**, 29–32.
4. Waku, Y., Ohtsubo, H., Nakagawa, N. and Kohtoku, Y., Sapphire matrix composites reinforced with single crystal YAG phases. *J. Mater. Sci.*, 1996, **31**, 4663–4670.
5. Waku, Y., Nakagawa, N., Wakamoto, T., Ohtsubo, H., Shimizu, K. and Kohtoku, Y., High-temperature strength and thermal stability of a unidirectionally solidified Al_2O_3/YAG eutectic composite. *J. Mater. Sci.*, 1998, **33**, 1217–1225.
6. Waku, Y., Nakagawa, N., Wakamoto, T., Ohtsubo, H., Shimizu, K. and Kohtoku, Y., The creep and thermal stability characteristics of a unidirectionally solidified Al_2O_3/YAG eutectic composite. *J. Mater. Sci.*, 1998, **33**, 4943–4951.
7. Bahlawane, N., Watanabe, T., Waku, Y., Mitani, A. and Nakagawa, N., Effect of moisture on the high-temperature stability of unidirectionally solidified Al_2O_3/YAG eutectic composites. *J. Am. Ceram. Soc.*, 2000, **83**, 3077–3081.
8. Nakagawa, N., Waku, Y., Wakamoto, T., Ohtsubo, H., Shimizu, K. and Kohtoku, Y., high temperature properties and thermal stability of a unidirectionally solidified $Al_2O_3/Er_3Al_5O_{12}$ eutectic composite. *J. Jpn. Inst. Met.*, 2000, **64**, 101–107.
9. Waku, Y., Nakagawa, N., Wakamoto, T., Ohtsubo, H., Shimizu, K. and Kohtoku, Y., A ductile ceramics eutectic composite with high strength at 1873 K. *Nature*, 1997, **389**, 49–52.
10. Frazer, C. S., Dickey, E. C. and Sayir, A., Crystallographic texture and orientation variants in Al_2O_3–$Y_3Al_5O_{12}$ directionally solidified eutectic crystals. *J. Cryst. Growth*, 2001, **233**, 187–195.
11. Mizutani, Y., Yasuda, H., Ohnaka, I., Maeda, N. and Waku, Y., Coupled growth of unidirectionally solidified Al_2O_3–YAG eutectic ceramics. *J. Cryst. Growth*, 2002, **244**, 384.
12. Mizutani, Y., Yasuda, H., Ohnaka, I., Maeda, T. and Waku, Y., Coupled growth zone of the Al_2O_3–YAG eutectic system in the undercooled melt. *J. Inst. Metals*, 2002, **66**, 9.
13. Yasuda, H., Mizutani, Y., Ohnaka, I. and Waku, Y., Production of the undercooled melt by heating the metastable Al_2O_3–YAP eutectic structure. *Mater. Trans.*, 2001, **42**, 1801–1807.
14. Yasuda, H., Mizutani, Y., Ohnaka, I., Sugiyama, A., Morikawa, T. and Waku, Y., Undercooled melt formation and shaping of Al_2O_3–YAG eutectic ceramics. *J. Am. Ceram. Soc.*, 2003, **86**, 1818–1820.
15. Caslavsky, J. L. and Viechnicki, D. J., Melting behaviour and metastability of yttrium aluminum garnet (YAG) and $YAlO_3$ determined by optical differential thermal analysis. *J. Mater. Sci.*, 1980, **15**, 1709–1718.
16. Yasuda, H., Ohnaka, I., Mizutani, Y., Maeda, N. and Waku, Y., Eutectic solidification of the Al_2O_3–Y_2O_3 ceramic system. In *Proceedings of the M.C. Flemings Symposium*. TMS, Boston, 2000, pp. 171–176.
17. Yasuda, H., Ohnaka, I., Mizutani, Y. and Waku, Y., Selection of eutectic systems in Al_2O_3–Y_2O_3 ceramics. *Sci. Tech. Adv. Mater.*, 2001, **2**, 67–71.
18. Mizutani, Y., Yasuda, H., Ohnaka, I. and Waku, Y., Phase selection of the Al_2O_3–Y_2O_3 system controlled by nucleation. *Mater. Trans.*, 2001, **42**, 238–244.
19. Uesugi, K., Suzuki, Y., Yagi, N., Tsuchiyama, A. and Nakano, T., Development of high spatial resolution X-ray CT system at BL47XU in SPring-8. *Nucl. Instrum. Methods Phys. Res.*, 2001, **A467–A468**, 853.
20. Salvo, L., Cloetens, P., Marie, E., Zabler, S., Blandin, J. J., Buffiere, J. Y. *et al.*, X-ray micro-tomography an attractive characterisation technique in materials science. *Nucl. Instrum. Methods Phys. Res. B*, 2003, **200**, 273–286.
21. Yasuda, H., Mizutani, Y., Ohnaka, I., Kirihara, M. and Sakimura, T., Application of an optical DTA for morphological transition in the

Al_2O_3–YAP–ZrO_2 metastable eutectic system. *ISIJ Int.*, 2003, **43**, 1733–1741.
22. Yasuda, H., Ohnaka, I., Mizutani, Y., Sugiyama, A., Morikawa, T., Takeshima, S. *et al.*, Shape casting of Al_2O_3–YAG eutectic ceramics by using the undercooled melt formation. *Sci. Technol. Adv. Mater.*, 2004, **5**, 207–217.
23. Yoshikawa, A., Epelbaum, B. M., Hasegawa, K., Durbin, S. D. and Fukuda, T., Microstructures in oxide eutectic fibers grown by a modified micro-pulling-down method. *J. Cryst. Growth*, 1999, **205**, 305–316.
24. Jackson, K. A. and Hunt, J. D., Lamellar and rod eutectic growth. *Trans. Metall. AIME*, 1966, **236**, 1129–1142.
25. Kurz, W. and Fisher, D. J., Dendrite growth in eutectic alloys: the coupled zone. *Int. Met. Rev.*, 1979, **24**, 177–204.
26. Kurz, W. and Fisher, D. J., Fundamentals of solidification. *Trans. Tech.*, 1989, 93–115.
27. Elliott, R., Eutectic solidification. *Int. Met. Rev.*, 1977, **22**, 161–186.
28. Yasuda, H., Ohnaka, I., Tsuchiyama, A., Nakano, T. and Uesugi, K., in preparation.
29. Allen, D. R., Gremaud, M. and Perepezko, J. H., Nucleation-controlled microstructural development in Al–Si alloys. *Mater. Sci. Eng.*, 1997, **A226–A228**, 173–177.
30. Pierantoni, M., Gremaud, M., Magnin, P., Stoll, D. and Kurz, W., The coupled zone of rapidly solidified Al–Si alloys in laser treatment. *Acta Metall. Mater.*, 1992, **40**, 1637–1644.